

ANISOTROPIC PROPAGATION CHARACTERISTICS OF ACOUSTIC EMISSION SIGNALS IN WOOD

YONGCHUAN WU¹, SAIYIN FANG¹, MING LI², TINGTING DENG¹, CHUMIN CHEN¹,
ZHIYINGTIAN¹

¹SOUTHWEST FORESTRY UNIVERSITY, CHINA

²ANHUI POLYTECHNIC UNIVERSITY, CHINA

RECEIVED APRIL 2025

ABSTRACT

This study investigates the propagation characteristics of acoustic emission (AE) signals in *Zelkova schneideriana* and *Pinus sylvestris* var. mongolic along different directions, with a focus on amplitude and frequency variations. Sinusoidal signals ranging from 10 to 400 kHz, along with pulsed signals of 1 μ s width and 1 s period, were generated using an arbitrary waveform generator to simulate the AE source. Experiments were conducted on 80 mm cubic wood specimens, with the AE source and sensors positioned at the geometric centers of each surface. AE signals were recorded at a sampling rate of 2 MHz. The results indicate that, at the same frequency, the *Zelkova schneideriana* exhibits higher signal amplitude and energy than the *Pinus sylvestris* var. mongolic. Frequency response analysis further reveals that wood enhances the propagation of signals below 75 kHz, while significantly attenuating signals above 200 kHz in the transverse direction.

KEYWORDS: *Zelkova schneideriana*, *Pinus sylvestris*, acoustic emission, low-frequency, frequency response.

INTRODUCTION

When a material is subjected to an external or internal force, the localized source transitions to a low-energy steady state by rapidly releasing energy, a phenomenon known as acoustic emission (AE) that releases strain energy by generating transient elastic waves (Vun et al. 2005), which is essentially an elastic wave with different modes and frequencies (Kundu et al. 2007; Wilcox 2005; Liu et al. 2014). Acoustic emission technology (AET), as a high-sensitivity dynamic nondestructive testing method, can monitor the test object in real

time without destroying it, and evaluate the fatigue cracking (Bhuiyan et al. 2018), energy attenuation (Wang et al. 2015) and other characteristics of the material.

In recent years, AET has also been widely used in the field of wood science (Aguilera & Zamora 2007; Kowalski & Smoczkiwicz 2003; Nasir & Cool 2020). Mao et al. (2022) established a model for energy attenuation of AE signals in the grain direction and explored the effects of frequency on signal amplitude and energy attenuation. Denget al. (2021) investigated AE signal features and propagation velocity using short-wave analysis and EMD methods, revealing the velocity change characteristics of wood as an anisotropic material. Wang et al. (2021) examined the influence of structural changes on stress wave propagation and analyzed the frequency spectrum characteristics of signals in solid and gaseous media. Zhanget al. (2021) analyzed the propagation rules of AE signals in live logs of the *Pinus yunnanensis* and studied the energy attenuation characteristics when AE signals propagate over different distances. Chen et al. (2024) described the velocity and energy changes of AE signals propagating in different directions on the sample surface, elucidating energy attenuation patterns. Song et al. (2020) investigated the relationship between AE signals microstructure and anisotropy in coal, finding that accumulated absolute energy changes with increasing anisotropy angles show a U-shaped pattern. Fenget al. (2010) investigated the propagation process of stress waves in wood, examining the relationship between the elastic constants of wood and the propagation characteristics of stress waves. They proposed a model for stress wave propagation based on the assumption of orthogonal anisotropy. Zhai et al. (2021) investigated the effect of axial compression load on the vibration and acoustic response characteristics of soundboard wood. Their findings revealed a regular effect of compression load on the vibration and acoustic properties of wood. Shen et al. (2006) investigated the strong correlation between longitudinal and radial vibration parameters of wood. They illustrated the longitudinal and radial vibration characteristics and calculated the vibration parameters. Eslami et al. (2021) proposed a constitutive model for simulating the nonlinear mechanical responses of wood as a plasticity-positive anisotropic material under three-dimensional stress conditions, pointing out that the constitutive relationships of wood differ between tension and compression states. Fuet al. (2025) elucidated the fundamental structural characteristics of wood elasticity and compressibility, spanning from the molecular to the macroscopic level. They further examined the relationship between these characteristics and the assembly patterns of lignocellulosic components in wood, as well as the helical arrangement of cell walls and their anisotropic properties.

The majority of extant studies on the propagation characteristics of wood based on AET focus on the study of propagation characteristics such as energy and velocity in the plane. However, as a porous material with significant orthogonal anisotropy, the propagation characteristics of wood in the longitudinal and transverse directions may also be different. Most existing studies investigating the propagation characteristics of AE signals in wood utilize the pencil-lead break (PLB) technique as the AE source. However, AE signals generated by PLB contain complex frequency components, which complicates the precise characterization of the attenuation behavior across different frequency bands. Therefore, this paper analyzes the propagation characteristics of wood in various directions under AE signals of different frequencies, based on the signal generator. Additionally, it explores the amplitude

and energy of AE signals across different types of wood at varying frequencies. In this paper, a single-channel arbitrary waveform generator is utilized to generate continuous sinusoidal and pulse signals to simulate the AE source. *Zelkova schneideriana* (hardwood) and *Pinus sylvestris* var. *mongolica* (softwood) are employed as the test materials. AE signals are collected by arranging them in the center of the specimen surfaces to explore the amplitudes and energies of AE signals of different frequencies in the *Zelkova schneideriana* and the *Pinus sylvestris* var. *mongolica*, as well as the frequency distributions of the wood to the pulse signals.

MATERIALS AND METHODS

Experimental material

In this study, two species of specimens were selected for analysis: *Zelkova schneideriana* and *Pinus sylvestris* var. *mongolic*. The specimens were free of surface defects and exhibited straight grain. The dimensions of the specimens were measured at 80×80×80 mm. Before the experiment, the density of the wood was measured in accordance with the method outlined in GB/T 1933-2009, a standard method for determining wood density. To facilitate the ensuing discussion, the specimens were defined as T1-T3 and their relevant parameters were listed in Tab. 1, in which the wood density was the measured value before the experiment.

The AE signal acquisition system was constructed using LabVIEW software and NI USB-6366 high-speed acquisition card. The AE sensor used was the single-ended resonant RS-2A sensor, with a frequency range of 50 kHz to 400 kHz, to enable long-distance transmission of AE signals, each channel was equipped with a 40 dB preamplifier to amplify the collected AE signals. The voltage range of the signal was set to (-10V, 10V). According to the Shannon sampling theorem, the sampling frequency is set to 2 MHz to observe the effect of wood on the frequency of the AE signals as comprehensively as possible. During the experimental process, the specimen and the sensor were filled with high-temperature insulating silicone grease to ensure full coupling between the specimen and the sensor, to minimize the influence of the air medium, and to improve the conduction efficiency of the sensor.

Tab. 1: The specific parameters of the specimen.

Test pieces	Material	Moisture content (%)	Wood density (kg/cm ³)
T1	<i>Zelkova schneideriana</i>	11.2	0.752
T2	Sapwood of <i>Pinus sylvestris</i> var. <i>mongolica</i>	11.4	0.512
T3	Heartwood of <i>Pinus sylvestris</i> var. <i>mongolica</i>	11.5	0.527

To facilitate the description, a three-dimensional rectangular coordinate system was established with the center of the cube specimen, as illustrated in Fig. 1a. In this coordinate system, the external normal direction of the wood cross-section is defined as the Z-axis. The Z+ plane and the Z- plane represent the positive and negative orientations of the external normal vector along the Z axis, respectively. The direction of the Z-axis aligns with that of the wood grain (longitudinally). The X-axis and Y-axis correspond to transverse texture directions within the specimen. The outer normal directions for radial sections of wood are designated as

negative X axis and negative Y axis, respectively. An orientation diagram for specimen T1 is presented in Fig. 1b, the direction of the annual ring is shown in Fig. 1c. It should be noted that specimens T2 and T3 exhibit an orientation consistent with that of specimen T1.

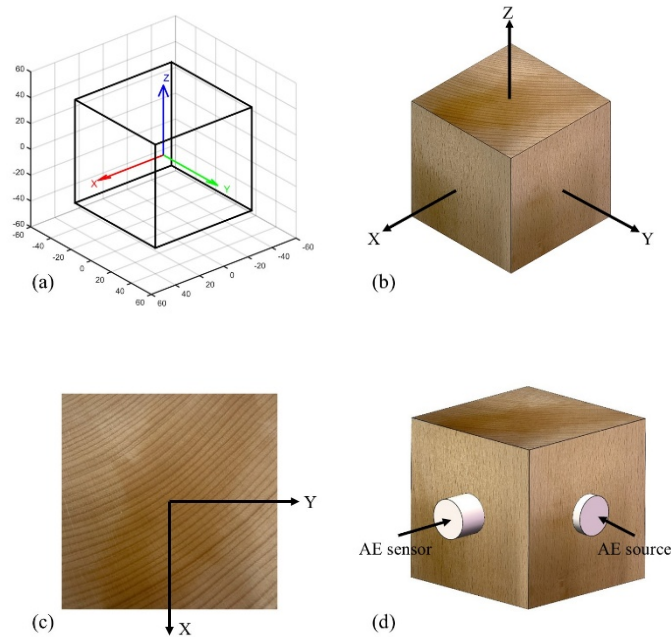


Fig. 1: Schematic diagrams of wood specimens: (a) Orientation of wood specimen, (b) The direction of T1 specimen, (c) Annual ring orientation of T1 specimen, (d) Test diagram of T1 specimen.

Test methods

To investigate the frequency variation of AE signals in various directions across different types of wood, an experimental scheme was accompanied by the test diagram depicted in Fig. 1d. In the experiment, an arbitrary waveform generator was employed to produce continuous sinusoidal and pulse signals, simulating the AE source. The energy of the AE source is controlled by adjusting the output voltage level. This AE source was positioned at the geometric center of one surface of a wood specimen. An AE sensor was then placed at the geometric center of the remaining surfaces of the specimen to collect AE signals. This procedure was repeated until measurements were obtained from all surfaces. The frequency of the continuous sinusoidal signal was incrementally increased from 10 kHz to 400 kHz in 10 kHz steps, while the single pulse width of the pulsed signal was fixed at 1 μ s with a pulse period of 1 s. In this experiment, the inverse piezoelectric effect of the piezoelectric ceramic sheet is exploited to generate signals at different frequencies as a simulated AE source, and the sinusoidal and pulsed signals are collected to analyze the propagation characteristics.

RESULTS AND ANALYSIS

Analysis of sinusoidal signals

The generation and change of the AE signals reflect the damage mechanism of the material. Various basic parameters such as amplitude and energy are extracted from the acoustic emission

signals to characterize the damage from different angles. In this paper, an arbitrary waveform generator is utilized to generate continuous sinusoidal signals at varying frequencies as the AE source to investigate the response of the wood structure in terms of the amplitude of sinusoidal signals at different frequencies. Initially, the amplitude response of the sensor to sinusoidal signals of varying frequencies was determined. The sensor was then placed in direct contact with the piezoelectric ceramics. Sinusoidal signals with frequencies ranging from 10 kHz to 400 kHz were captured as the excitation signals. The sinusoidal signals were subsequently applied to the centers of the different surfaces of the wood. As illustrated in Tab. 2, the designation Z⁺-Y⁺ signifies that the AE source has been positioned in the Z⁺ plane, while the sensor has been placed in the Y⁺ plane to facilitate the reception of the AE signal.

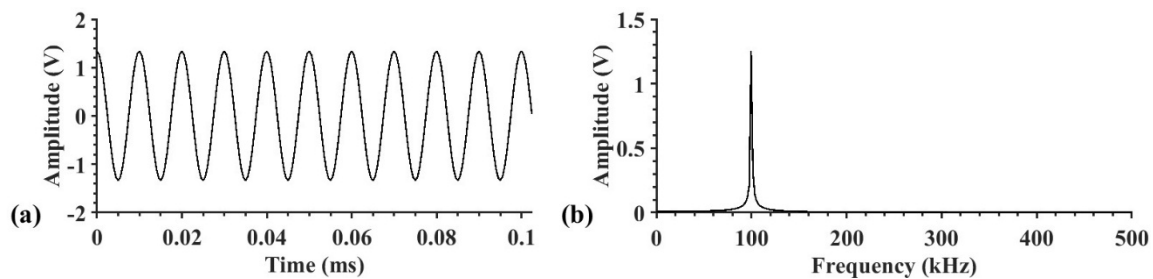


Fig. 2: Sinusoidal signal. (a) AE waveforms, (b) Frequency spectrum.

Tab. 2: The amplitude of the sinusoidal signal in different directions of the wood.

Test pieces	Amplitude (V)				
	Z ₊ - Y ₊	Z ₊ - Y ₋	Z ₊ - Z ₋	Z ₊ - X ₊	Z ₊ - X ₋
T1	1.346	1.315	8.283	0.668	1.375
T2	0.464	0.751	8.052	1.003	0.423
T3	1.735	2.005	7.953	0.735	1.014

Under sinusoidal excitation, the AE output signal maintains a sinusoidal pattern after attaining a steady state in various propagation directions of the wood, both in *Zelkova schneideriana* and *Pinus sylvestris* var. Mongolic (Fig. 2). The frequency of the AE output signal is consistent with that of the input signal. Tab. 2 presents the amplitudes of the three wood specimens in various propagation directions under 100 kHz sinusoidal excitation. The amplitude of the AE signal in the longitudinal direction (Z-axis direction) approaches 8 V, while the amplitudes in the other directions range from 1 V to 2 V. This finding suggests that the AE signal exhibits a higher response strength during propagation in the longitudinal direction. Wood, as a kind of orthotropic anisotropic material, has an obvious difference in the propagation characteristics of the AE signal in different directions. This phenomenon is because the structure and cell arrangement of wood are closely related to the signal propagation. Specifically, in the longitudinal direction, the cellular fibers of wood are neatly aligned, and the conduit and fiber orientations of wood are consistent with the grain direction. This allows the signal to propagate along the tightly aligned paths between the wood fibers, reducing the energy attenuation during signal propagation. Consequently, the AE signal intensity is higher in the longitudinal direction. In contrast, in the transverse direction, the propagation path of the AE signal is more complex. Wood exhibits substantial interstitial spaces between cell walls in this orientation, and tissues such as wood rays demonstrate

irregular alignment in this direction, resulting in a tortuous signal propagation path and greater energy dissipation, which consequently leads to a comparatively diminished AE signal amplitude.

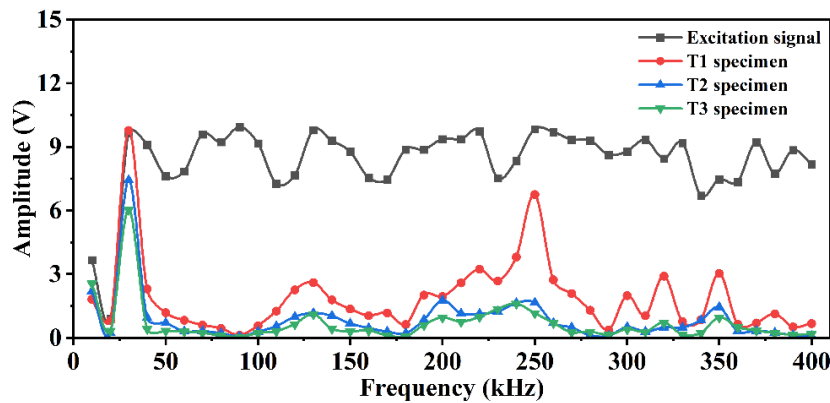


Fig. 3: Amplitude of sinusoidal signals with different frequencies for different woods.

Fig. 3 shows the amplitude of the AE signal in the longitudinal direction of the wood at various frequencies. The findings indicate that the amplitude of the T1 specimen exceeds that of the T2 and T3 specimens at equivalent frequencies. Moreover, while the amplitude curves of the T2 and T3 specimens exhibit similarities, the amplitude of the AE signal for T2 surpasses that of T3 within the range of 10 kHz to 200 kHz. This is because the density and elastic modulus of *Zelkova schneideriana* are both higher than those of *Pinus sylvestris* var. *mongolica*, and the elastic modulus of wood primarily depends on its fiber structure rather than density (Tu & Shao 2012). When AE signals pass through *Zelkova schneideriana*, its dense structure and uniform pore and fiber arrangement result in a relatively direct transmission path with less energy concentration and lower propagation loss. Conversely, *Pinus sylvestris* var. *mongolica*, characterized by its relatively loose fiber structure, exhibits a more dispersed stress distribution when subjected to force, resulting in a smaller energy of the AE signal. The AE signal traverses the *Pinus sylvestris* var. *mongolica* with a more circuitous and weakened trajectory due to its lax structure, elevated porosity, and resin canal. This renders it susceptible to scattering and reflection. Consequently, the amplitude of AE signals from the T1 specimen with varying frequencies exceeds that of AE signals from the T2 and T3 specimens. Within the frequency range of 10 kHz to 200 kHz, the amplitude of AE signals in T2 was slightly higher than that in T3. This is attributed to the inverse relationship between wood density and annual ring width in softwoods (Boccacci et al. 2022). The wider annual rings and looser structure of the sapwood result in fewer acoustic impedance interfaces along the propagation path, thereby reducing scattering and reflection and preserving higher signal amplitudes. In contrast, the narrower annual rings and denser structure of the heartwood introduce more interfaces, causing repeated energy dissipation during propagation and a corresponding decrease in signal amplitude.

To facilitate the analysis of AE signals through wood, the amplitude attenuation law must be considered, as well as the amplitude of the excitation signal at different frequencies and the amplitude of the sinusoidal signal through the wood. The ratio of the amplitude of the signal to determine the amplitude attenuation law is critical. The degree of amplitude attenuation of

the indicators is determined by the amplitude residual percentage, a (Chen et al. 2025). A larger ratio indicates a slower rate of AE signal attenuation, reflecting a reduced loss of signal strength:

$$a = \frac{A_i}{A_0} \quad (1)$$

where: A_i is the AE signal amplitude of the wood specimens, and A_0 is the AE signal amplitude of the excitation.

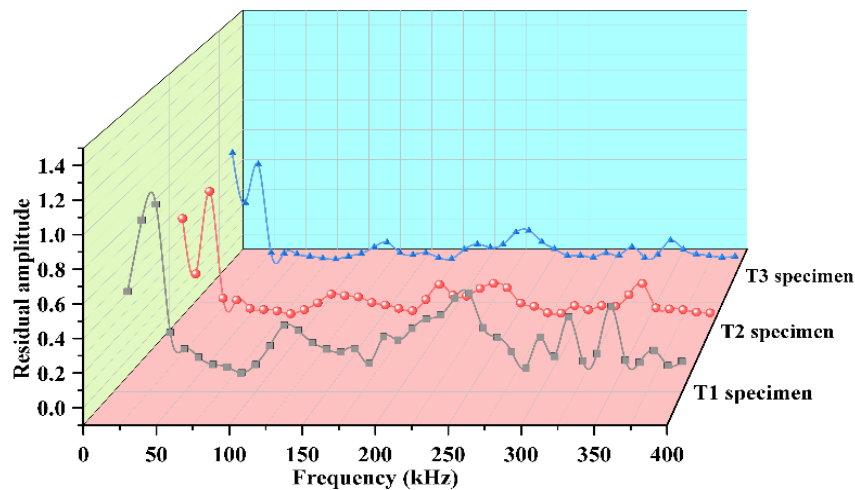


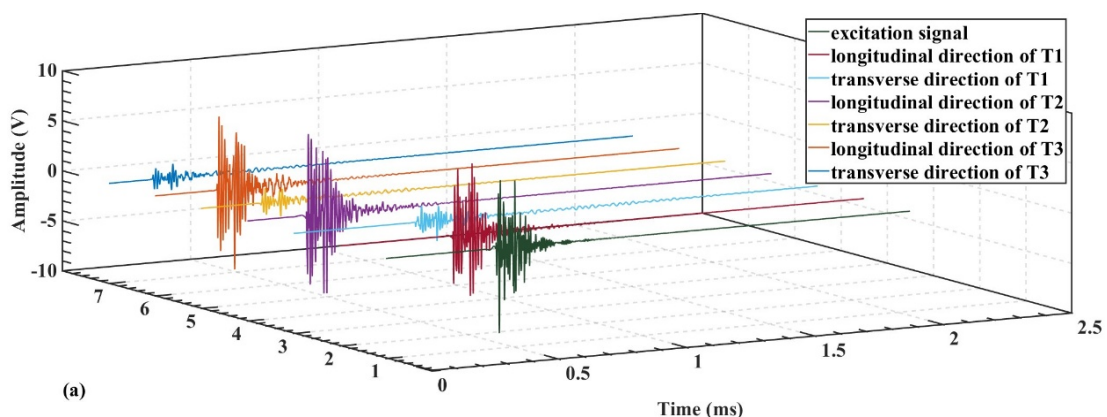
Fig. 4: Curves of the residual amplitude of different wood specimens.

The present study examined the trend of the amplitude residual percentage of the AE signals in the wood in the longitudinal direction. This analysis was conducted according to Eq. 1, as illustrated in Fig. 4. The results demonstrated that, within the frequency range of 10 kHz to 100 kHz, the amplitude residual percentage of the three specimens exhibited a decreasing trend with increasing frequency. In the range of 100 kHz to 400 kHz, the amplitude residual percentage of the T2 and T3 specimens exhibited a tendency to be relatively stable and flat, while the fluctuation of the T1 specimen was more pronounced. For frequencies below 80 kHz, the amplitude residual percentage a was significantly larger than for frequencies above 80 kHz. This observation signifies that the decay rate of signals below 80 kHz is slower in the direction of the grain, while signals above 80 kHz decay faster. The decay rate of AE signals propagating along the wood in the longitudinal direction is frequency-dependent, with higher-frequency signals decaying at a faster rate (Wang et al. 2010). This phenomenon can be attributed to the filtering effect of the porous structure and viscoelasticity of wood on AE signals within a specific frequency band. When a stress wave propagates through a viscoelastic medium, viscoelasticity emerges as the predominant factor leading to stress wave attenuation in space and over time. Consequently, the high-frequency component of AE signals experiences faster attenuation compared to the low-frequency component within the wood.

Analysis of pulse signals

The procedure for the sinusoidal signal test was replicated, employing a pulse signal from an arbitrary waveform generator as the AE source. The individual pulse width was set to 1 μ s, and the pulse period was set to 1 s. The pulse signal was positioned at the center of the specimen surface. Initially, the sensor was placed in direct contact with the piezoelectric ceramic, and the AE signal excited by the pulse signal was collected as the excitation signal. Tests were conducted by applying the pulse signal at the geometric centers of different surfaces of the wood. The results are displayed in Fig. 5. In these figures, the term "longitudinal direction" indicates that the AE source is positioned in the Z_+ plane, while the sensor receiving the AE signal is situated in the Z plane. Conversely, "transverse direction" signifies that the AE source is placed in the Y_+ plane, with the sensor receiving the AE signal positioned in the Y plane.

The waveforms of AE signals contain rich characteristic information, and the spectral characterization of AE signals can reveal the characteristic laws of AE source more comprehensively and accurately. However, the AE signals collected in practice are often mixed with noise, which affects the analysis results. For this reason, this paper adopts the wavelet analysis method to denoise the AE signal. The wavelet analysis method is capable of decomposing the signal into sub-signals of varying frequency bands, and selecting the components that accurately reflect the true AE signal through the time-frequency characteristics of each frequency band for reconstruction, thereby achieving signal denoising (Ju et al. 2018). To enhance the frequency domain localization capability of wavelet analysis, the Daubechies 10 (db10) wavelet is employed as the wavelet basis function for 6-layer decomposition, ensuring coverage of the frequency response range of the sensor. The frequency bands of the high-frequency detailed signals in each layer are as follows: d1 (500 kHz~1000 kHz), d2 (250 kHz~500 kHz), d3 (125 kHz~250kHz), d4 (62.5 kHz~125 kHz), d5 (31.25 kHz~62.5 kHz), and d6 (15.625 kHz~31.25 kHz). According to the time-frequency characteristics of the signals in each layer, layers 3, 4, and 5 are selected to reconstruct the AE signals collected by the sensors. The waveforms and spectra of the reconstructed AE signals are shown in Fig. 5.



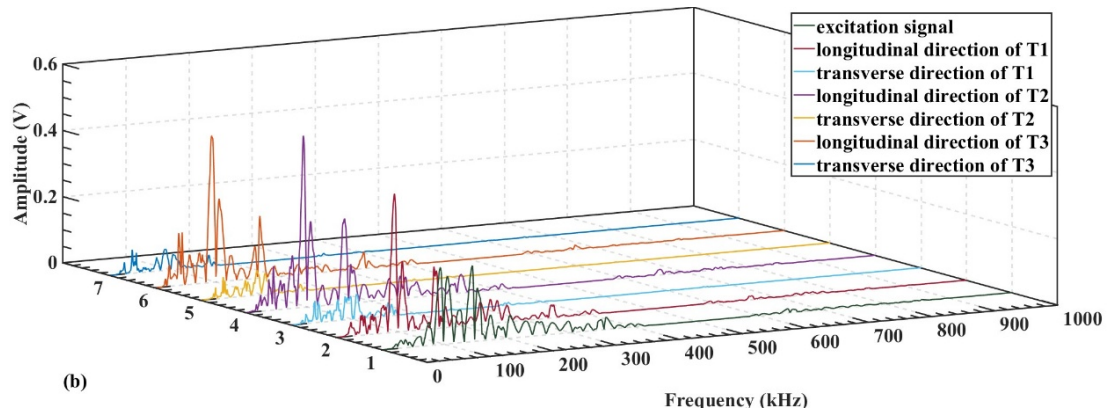


Fig. 5: Variation of AE waveforms and frequency spectrums. (a) Reconstructed AE waveforms, (b) Frequency spectrum.

As illustrated in Fig. 5a, the amplitude of the AE signal in the longitudinal direction is significantly higher than that in the transverse direction, which is about 8 V, while the amplitude of the signal in the transverse direction is only 1.5 V. The pulse amplitude of the longitudinal signal is large, the initial impact is strong, the energy is concentrated and attenuated rapidly, and it shows obvious damping characteristics. The amplitude of the transverse signal is small, the oscillation is significant and the attenuation is slow, the tail oscillation duration is long, the reflection signal is obvious, and the energy distribution is relatively dispersed. As a result, the longitudinal signal has a stronger initial shock and energy concentration, indicating less energy loss during propagation, while the transverse signal has a longer oscillation tail and energy dispersion, reflecting greater energy dissipation in the propagation path.

As illustrated in Fig. 5b, the excitation signal exhibits a distinct distribution within the range of 0 kHz to 400 kHz, while the distribution between 400 kHz and 1000 kHz is less pronounced. The amplitude of the excitation signal can reach up to 0.1V, corresponding to frequencies of 93 kHz and 140 kHz. The primary frequency of the AE signal propagating in the wood in the longitudinal direction is approximately 92 kHz, and the secondary frequency is approximately 155 kHz. In contrast, in the transverse direction, the frequency distribution is more homogeneous, with higher energies at 38 kHz, 92 kHz, and 104 kHz. As illustrated in Fig. 6, by comparing the frequency of the AE signal after propagation through the wood with the frequency of the excitation signal, it can be observed that the energy of the AE signal below 75 kHz is significantly enhanced in the longitudinal direction, whereas the energy of the AE signal is significantly attenuated at about 140 kHz, and signals higher than 200 kHz show a smaller attenuation. In the transverse direction, the energy of the AE signal is significantly enhanced below 75 kHz, while the attenuation is particularly significant and the signal energy is substantially reduced above 200 kHz.

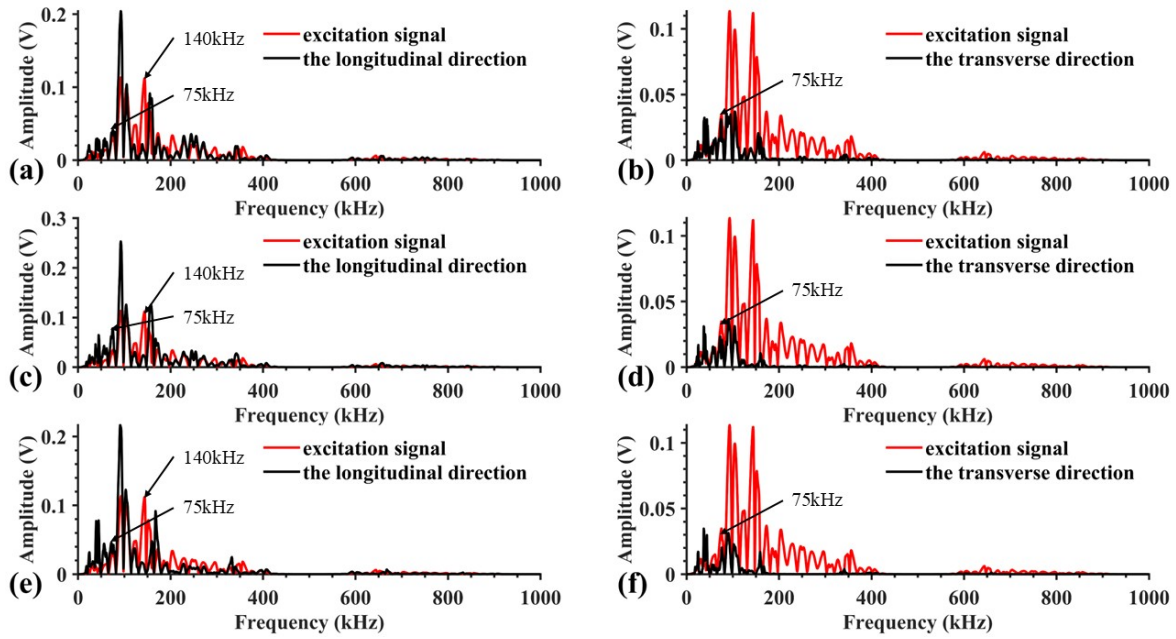


Fig. 6: Frequency-domain contrast diagram. (a) T1 with the longitudinal direction, (b) T1 with the transverse direction, (c) T2 with the longitudinal direction, (d) T2 with the transverse direction, (e) T3 with the longitudinal direction, (f) T3 with the transverse direction.

To facilitate the analysis of the frequency characteristics of AE signals propagating through wood, the wood specimen was treated as a system, and the frequency response function (FRF) was employed to characterize the energy distribution of AE signals across various frequencies. By elucidating the relationship between the input excitation signal and the output response signal, this study reveals the anisotropic properties of wood and their impact on AE signal propagation. The calculation formula is presented as follows:

$$H(\omega) = \frac{|Y(\omega)|}{|X(\omega)|} \quad (2)$$

where: $H(\omega)$ is the frequency response function, $X(\omega)$ is the Fourier transform of the excitation signal, and $Y(\omega)$ is the Fourier transform of the AE signal after passing through the wood.

The frequency response characteristics of the wood specimens can be obtained by spectral analysis of the AE input and output signals of the wood specimens to understand the response of the wood to different frequency components. As illustrated in Fig. 7, the three specimens exhibit multiple notable frequency response peaks within the 0 kHz to 100 kHz range, manifesting in both the longitudinal and transverse directions. This observation signifies that the AE signals undergo substantial energy enhancement within the low-frequency range. In the range of 100 kHz to 200 kHz, a significant peak emerges at approximately 160 kHz, corresponding to the resonance frequency of the AE sensor, as reported in a prior study (Xu et al. 2023). Above 200 kHz, the frequency response in the transverse direction exhibits several peaks. However, the frequency comparison analysis in Fig. 6 indicates that the AE signal is less distributed in the high frequency range.

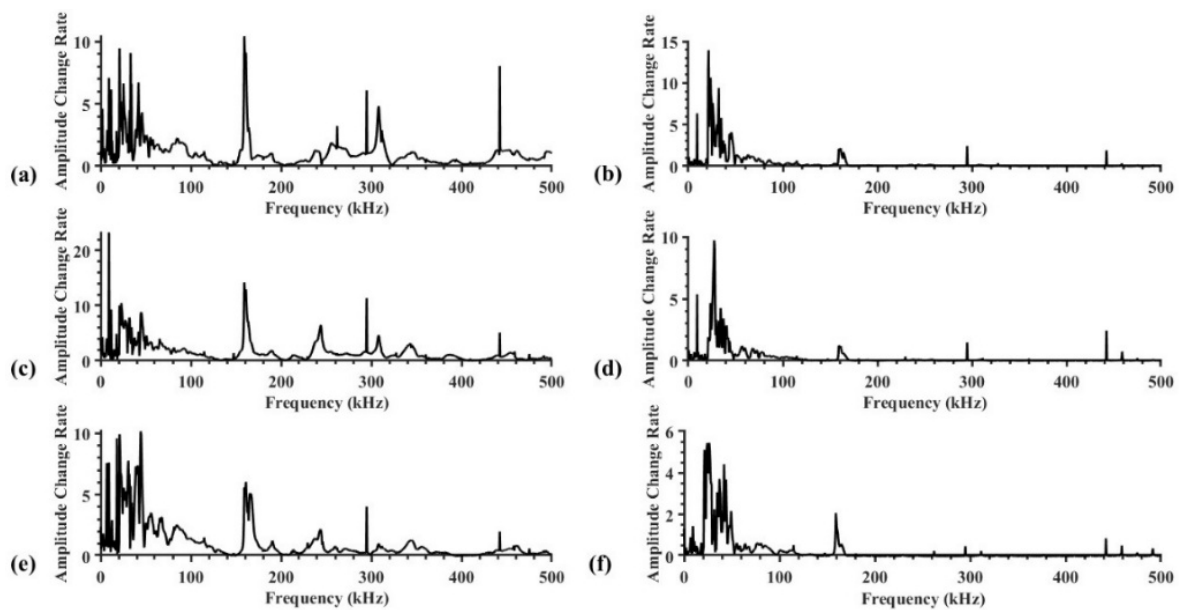


Fig. 7: Frequency response comparison diagram. (a) T1 with the longitudinal direction, (b) T1 with the transverse direction, (c) T2 with the longitudinal direction, (d) T2 with the transverse direction, (e) T3 with the longitudinal direction, (f) T3 with the transverse direction.

Furthermore, the frequency response in the transverse direction is virtually non-existent, suggesting that the propagation of the AE signal in the high-frequency phase is substantially suppressed. This finding indicates that, within the context of wood, low-frequency signals experience an enhancement in their intensity as they propagate through the material, while high-frequency signals demonstrate a greater propensity to undergo attenuation. This phenomenon can be attributed to the fact that high-frequency signals find it challenging to effectively penetrate the fiber structure of wood due to their shorter wavelengths. Consequently, these signals encounter greater diffraction, scattering, and reflection during propagation, resulting in a more rapid rate of attenuation (Yu et al. 2023). Consequently, both in the amplitude residual percentage and in the spectral comparison analysis, it can be observed that the AE signals propagate through the wood with a greater attenuation of the high-frequency AE signal losses and a smaller attenuation of the low-frequency signals.

CONCLUSIONS

In this experiment, an arbitrary waveform generator is used to generate sinusoidal signals of different frequencies and pulse signals of the same pulse width to simulate the generation of an AE source. The experiment investigated the laws of amplitude and frequency of AE signals propagating in different directions along the *Zelkova schneideriana* and the *Pinus sylvestris* var. *mongolica*. The experiment also explored the effects of AE signals of different frequencies on the amplitude and frequency of different directions of the wood. The obtained results are as follows: (1) It is evident that the amplitude and energy of the AE signal undergo a corresponding alteration in accordance with the variation in frequency. A notable distinction

emerges in the amplitude and energy of the *Zelkova schneiderian* when compared with those of the *Pinus sylvestris* var. *mongolica*, particularly in the direction of wood longitudinal and at a constant frequency. (2) When AE signals propagate in the wood in different directions, the wood specimens exhibit evident filtering characteristics in various orientations. The FRF curves demonstrate that the wood exhibits notable energy enhancement for AE signals below 75 kHz in both the longitudinal and transverse directions. However, in the transverse direction, signals exceeding 200 kHz encounter significant attenuation, suggesting a pronounced capacity to suppress high-frequency signals. Consequently, wood demonstrates a heightened capacity to propagate low-frequency signals (below 75 kHz).

This paper explores the impact of various directions of distinct wood types on the energy and amplitude of AE signals at different frequencies. The experimental results demonstrate that the *Zelkova schneiderian* and the *Pinus sylvestris* var. *mongolica* with varying orientations exhibit discernible filtering characteristics in the frequency domain of AE signals. Specifically, wood samples with the longitudinal direction exhibit a reduced effect on the high-frequency portion of AE signals, while those with the transverse direction exhibit a significant inhibition of the high-frequency portion of the AE signals. This paper focuses exclusively on the impact of varying frequency AE signals on the magnitude and frequency fluctuations when these signals propagate along diverse orientations in wood. Subsequent studies can expand the scope of the study and further divide the wood into coniferous wood, ring-porous deciduous wood, and scattered-porous deciduous wood. The analysis of the propagation characteristics of AE signals between different tree species and variant tree species will help to gain a deeper understanding of the topics involved in this study.

ACKNOWLEDGEMENTS

This work was supported by the Yunnan Agricultural Joint Special Project (202501BD070001-030, 202401BD070001-121), the National Natural Science Foundation of China (32160345, 31760182), the Startup fund for introducing talents and scientific research of Anhui University of Engineering (2021YQQ037), the Yunnan Key Service Industry Science and Technology Project (FWCY-BSPY2024099).

REFERENCE

1. Aguilera, A., & Zamora, R. (2007). Monitoreo del proceso de maquinado de aroma australiano (*Acacia melanoxylon*) con emisión acústica y su relación con la calidad superficial resultante. *Maderas. Ciencia y Tecnología*, 9(3).
2. Bhuiyan, M. Y., Lin, B., & Giurgiutiu, V. (2018). Acoustic emission sensor effect and waveform evolution during fatigue crack growth in thin metallic plate. *Journal of Intelligent Material Systems and Structures*, 29(7), 1275–1284.
3. Boccacci, G., Frasca, F., Bertolin, C., & Siani, A. M. (2022). Influencing factors in acoustic emission detection: A literature review focusing on grain angle and high/low tree ring density of scots pine. *Applied Sciences*, 12(2), 859.

4. Chen, C., Li, M., Fang, S., & Zhang, B. (2024). Anisotropic velocity model and energy attenuation characteristics of acoustic emission signals in finger-jointed timber and sawn timber. *Wood Research*, 69(4), 597–610.
5. Chen, C., Li, M., Fang, S., Zhao, J., Shen, Z., Zhang, Z., & Deng, T. (2025). Influence of acoustic emission technology on the energy attenuation characteristics of stress waves related to surface cracks in wood. *Forest Engineering*, 41(1), 40–49.
6. Deng, T., Ju, S., Wang, M., & Li, M. (2021). Study on propagation law of acoustic emission signals on anisotropic wood surface. *Wood Research*, 66(4), Article 4.
7. Eslami, H. (2021). Nonlinear three-dimensional anisotropic material model for failure analysis of timber. *Engineering Failure Analysis*.
8. Feng, H., Li, G., Fang Y., & Li, J. (2010). Stress wave propagation model and its application in wood detection. *Journal of System Simulation*, 22(6), Article 6.
9. Fu, Z., Lu, Y., Wu, G., Bai, L., Barker-Rothschild, D., Lyu, J., Liu, S., & Rojas, O. J. (2025). Wood elasticity and compressible wood-based materials: Functional design and applications. *Progress in Materials Science*, 147, 101354.
10. Han C., Yang G., Wang J., & Guo X. (2020). The research on propagation characteristics of acoustic emission signals in stiffened plates based on the multipath propagation model. *Ultrasonics*, 108, 106177.
11. Ju, S., Li, X., Luo, T., & Li, M. (2018). Characteristics of acoustic emission signals on the surface of masson pine gulum with wavelet analysis method. *Journal of Northeast Forestry University*, 46(8), Article 8.
12. Kowalski, S., & Smockiewicz, A. (2003). Identification of wood destruction during drying. *Maderas. Ciencia y Tecnología*, 6.
13. Kundu, T., Das, S., & Jata, K. V. (2007). Point of impact prediction in isotropic and anisotropic plates from the acoustic emission data. *The Journal of the Acoustical Society of America*, 122(4), Article 4.
14. Liu, P., Chen, S., Guo, Y., & Li, P. (2014). Moment tensor inversion of acoustic emission. *Chinese Journal of Geophysics*, 57(3): 858-866
15. Mao, F., Fang, S., Li, M., Huang, C., Deng, T., Zhao, Y., & Qin, G. (2022). Study on attenuation characteristics of acoustic emission signals with different frequencies in wood. *Sensors*, 22(16), Article 16.
16. Nasir, V., & Cool, J. (2020). Characterization, optimization, and acoustic emission monitoring of airborne dust emission during wood sawing. *International Journal of Advanced Manufacturing Technology*, 109(9–12), 2365–2375.
17. Shen, J. (2006). Study on the relationships between longitude and radial sound vibration parameters of genus picea. *Scientia Silvae Sinicae*, 42(3): 21-24.
18. Song, H., Zhao, Y., Elsworth, D., Jiang, Y., & Wang, J. (2020). Anisotropy of acoustic emission in coal under the uniaxial loading condition. *Chaos, Solitons & Fractals*, 130, 109465.
19. Tu, D., & Shao, Z. (2012). Influence of wood density on acoustic vibration characteristic parameters. *Journal of Anhui Agricultural University*, 39(3), 361-364.
20. Vun, R. Y., deHoop, C., & Beall, F. C. (2005). Monitoring critical defects of creep rupture in oriented strandboard using acoustic emission: Incorporation of EN300 standard. *Wood Science and Technology*, 39(3), 199–214.

21. Wang, G., Li, C., Hu, S., Feng, C., & Li, S. (2010). A study of time- and spatial-attenuation of stress wave amplitude in rock mass. *Rock and Soil Mechanics*, 31(11), 3487–3492.
22. Wang, M., Deng, T., Li, X., Ding, R., Lai, F., Luo, R., & Li, M. (2021). Propagation Characteristics of Acoustic Emission Signals in L-Shaped Wood. *Journal of Northwest Forestry University*, 36(2), Article 2.
23. Wang, X., Xiang, J., Hu, H., Xie, W., & Li, X. (2015). Acoustic emission detection for mass fractions of materials based on wavelet packet technology. *Ultrasonics*, 60, 27–32.
24. Wilcox P. (2005). Application of guided wave signal processing to acoustic emission data. *AIP Conference Proceedings*, 760(1), 1809–1816.
25. Xu, N., Li, M., Fang, S., Huang, C., Chen, C., Zhao, Y., Mao, F., Deng, T., & Wang, Y. (2023). Research on the detection of the hole in wood based on acoustic emission frequency sweeping. *Construction and Building Materials*, 400, 132761.
26. Yu, A., Chen, Z., Wu, X., Mao, F., & Chen, X. (2023). Effect of concrete strength level on acoustic emission wave propagation characteristics. *Journal of Henan University of Science and Technology (Natural Science)*, 44(6), Article 6.
27. Zhang, Y., Deng, T., Li, S., Zhang, S., & He, Y. (2021). Acoustic emission signal propagation and attenuation of *Pinus yunnanensis*. *Mechanical Engineer*, 7, 74-76+82.

YONGCHUAN WU
SOUTHWEST FORESTRY UNIVERSITY
SCHOOL OF MACHINERY AND TRANSPORTATION
KUNMING, YUNNAN, CHINA

MING LI*
ANHUI POLYTECHNIC UNIVERSITY
¹KEY LABORATORY OF ADVANCED PERCEPTION AND INTELLIGENT CONTROL
OF HIGH-END EQUIPMENT OF MINISTRY OF EDUCATION
²SCHOOL OF ELECTRICAL ENGINEERING
WUHU, ANHUI, CHINA
*Corresponding author: swfu_lm@swfu.edu.cn

SAIYIN FANG*, TINGTING DENG, CHUMIN CHEN, ZHIYINGTIAN
SOUTHWEST FORESTRY UNIVERSITY
SCHOOL OF MACHINERY AND TRANSPORTATION
KUNMING, YUNNAN, CHINA
*Corresponding author: fsy029@126.com